Heliyon 10 (2024) e38014

Contents lists available at ScienceDirect

Heliyon

journal homepage: www.cell.com/heliyon

Research article

Exploring tumor microenvironment in molecular subtyping and prognostic signatures in ovarian cancer and identification of SH2D1A as a key regulator of ovarian cancer carcinogenesis

Hongrui Guo [a], liwen Zhang [b], Huancheng Su [a], Jiaolin Yang [a], Jing Lei [a], Xiaoli Li [b,**], Sanyuan Zhang [a,***], Xinglin Zhang [a,*]

[a] Department of Gynecology, First Hospital of Shanxi Medical University, Taiyuan, 030001, China
[b] Department of Gynecology, The Children's Hospital of Shanxi, Taiyuan, 030001, China

ARTICLE INFO

Keywords:
Ovarian cancer
Tumor microenvironment
Prognosis
Multi-omics
Machine learning
SH2D1A
Migration
Proliferation

ABSTRACT

Introduction: A deadly gynecological cancer, ovarian cancer (OV), has a poor prognosis because of late-stage diagnosis and few targeted therapies. Addressing the tumor microenvironment (TME) in solid tumors has shown promise since it is crucial in promoting cancer progression.

Methods: We obtained bulk RNA-seq data from TCGA-OV, GSE26712, GSE102073, and ICGC cohorts, as well as scRNA-seq data from EMTAB8107, GSE118828, GSE130000, and GSE154600 cohorts using the TISCH2 database. The ConsensusClusterPlus package was used to cluster the OV tumor tissues hierarchically to determine two molecularly different groups (C1 and C2). A total of ten different types of machine learning techniques with 101 combinations were used for prognostic model construction. Using eight TME algorithms integrated into the IOBR R package, the bulk RNA-seq dataset was analyzed. For in vitro experiments, OVCAR3 and SKOV3, two OV cell lines, were used. The migratory potential of the ovarian cancer cells was assessed using Transwell assay, while proliferation was assessed using CCK8 assay.

Results: Based on TME-related gene set expression, two distinct molecular subgroups (C1 and C2) were identified through consensus clustering, with C1 showing higher TME activity. Further analysis indicated that C1 had increased cancer-associated fibroblasts (CAFs), M1 macrophages, and $CD8^{+}$ T cells, suggesting a more activated and pro-inflammatory TME. Drug sensitivity analysis revealed that 5-Fluorouracil might be beneficial to C1 patients. Functional differences between C1 and C2 were identified, including cell adhesion, mononuclear cell differentiation, and leukocyte migration. A machine learning model was developed to create a TME-related prognostic signature, demonstrating strong prognostic capabilities across multiple datasets. High-risk patients showed a more immune-suppressive TME and higher tumor stemness. ScRNA-seq disclosed a highly activated TME-related signature in OV. Cancer cell lines had significantly higher SH2D1A mRNA expression than normal ovarian epithelial cells. We observed that SH2D1A knockdown in 2 ovarian cancer cell lines (OVCAR3 and SKOV3) reduced migration and proliferation through a series of in-vitro experiments.

Conclusion: TME-associated genes were efficient in ovarian cancer molecular subtyping. A TME-based prognosis model was constructed for vigorous prognostic stratification efficacy across

* Corresponding author. Department of Gynecology, First Hospital of Shanxi Medical University, Taiyuan, 030001, China.
** Corresponding author. Department of Gynecology, The Children's Hospital of Shanxi, Taiyuan, 030001, China.
*** Corresponding author. Department of Gynecology, First Hospital of Shanxi Medical University, Taiyuan, 030001, China.
E-mail addresses: Xiaoli-010@163.com (X. Li), zsyprofessor@aliyun.com (S. Zhang), xinglinyuan860807@163.com (X. Zhang).

https://doi.org/10.1016/j.heliyon.2024.e38014
Received 15 July 2024; Received in revised form 11 September 2024; Accepted 16 September 2024
Available online 17 September 2024

multiple datasets. Moreover, we identified a pivotal role of SH2D1A in promoting proliferation and migration in ovarian cancer.

1. Introduction

Global Cancer Statistics states that over 200,000 patients globally lost their lives to ovarian cancer (OV) [1]. OV is considered one of the deadliest gynecological malignancies. Due to a lack of distinguishing signs and symptoms, most patients get diagnosed during advanced stages, reducing survival rates [2,3]. The late-stage diagnosis and limited accuracy in early detection pose significant challenges. The overall five-year survival rate for ovarian cancer remains unsatisfactory despite significant advancements in treatment approaches such as surgery, radiation therapy, and chemotherapy [4–6]. However, the availability of suitable targeted therapies is still limited. It is urgent to investigate the molecular pathways and identify potential targets to improve the ovarian cancer diagnosis and treatment approach. It will ultimately improve patient outcomes and survival rates.

The tumor microenvironment (TME), which includes signaling molecules, extracellular matrix, tumor cells, and non-cancerous cells, is vital in driving cancer cell progression [7]. TME genes play a role through various pathways in the proliferation, survival, and immune evasion of tumor cells in multiple cancers, including breast, ovarian, lung, colorectal, prostate, and pancreatic cancers. Among these, TME genes regulate the secretion of cytokines that support tumor cell survival and proliferation, enhancing the aggressiveness of tumors. Additionally, interactions between ovarian cancer cells and surrounding stromal cells alter tumor behavior, including resistance to chemotherapy. TME genes are essential for the initiation, progression, and metastasis of multiple cancers, involving various aspects of cell progression, such as immune modulation, stromal interaction, angiogenesis, and extracellular matrix remodeling. Targeting the TME has become a more viable treatment option for solid tumors in recent years [8,9]. The landscape of cancer treatment has changed due to the development of immune checkpoint inhibitors (ICIs), which target pathways such as PD-1/PD-L1 and CTLA-4 [10–12]. Clinical trials employing ICIs as monotherapy or in combination with chemotherapy have not shown significant survival benefits in the case of ovarian cancer. This could be attributed to the complex and highly immunosuppressive nature of the OV TME. To overcome these obstacles, a deeper understanding of the relationships between OV tumor cells and their milieu is needed. Thus, further characterization and exploration of the OV TME may be key to improving therapeutic outcomes in OV patients. Muti-omics analysis and novel machine-learning approaches are useful in improving prognosis and untangling the intricate TME of multiple types of solid tumors [13–15]. Hence, we aimed to explore TME's role in ovarian cancer using computational analysis methods.

In this study, 4 TME-related gene sets were analyzed, revealing a heterogeneous expression pattern in the TME of ovarian cancer. Consensus clustering identified two distinct molecular subgroups (C1 and C2) based on TME scores, with C1 exhibiting higher TME activity. The immune infiltration study's findings showed that C1's TME was more active and pro-inflammatory than C2's, with C1 having more Cancer-associated fibroblasts (CAFs), M1 macrophages, and $CD8^+$ T cells. Drug sensitivity analysis revealed that C2 patients had a superior response to many drugs, while C1 patients may benefit more from 5-Fluorouracil. Functional differences were identified between C1 and C2, including cell adhesion, mononuclear cell differentiation, and leukocyte migration. The development of a TME-related prognostic signature by machine learning showed good prognostic ability across multiple datasets. High-risk patients had a more immune-suppressive TME and higher tumor stemness. Single-cell analysis identified different cell types and their associated gene expression patterns in the TME [16]. Comparing normal ovarian epithelial cells to cancer cell lines, the mRNA expression of SH2D1A was significantly higher. In vitro experiments on 2 ovarian cancer cell lines (OVCAR3 and SKOV3) showed decreased migration and proliferation with SH2D1A knockdown. Overall, the study provided insights into the TME in ovarian cancer, highlighting potential therapeutic strategies and prognostic markers. Moreover, we identified a pivotal role of SH2D1A in promoting proliferation and migration in ovarian cancer.

2. Methods

2.1. Sequencing data collection and processing

We enrolled bulk RNA-seq data of OV cancer patients from the TCGA-OV cohort (https://portal.gdc.cancer.gov/) using the TCGA bio links R package, GSE26712 (https://www.ncbi.nlm.nih.gov/geo/query/acc.cgi?acc=GSE26712) and GSE102073 (https://www.ncbi.nlm.nih.gov/geo/query/acc.cgi?acc=GSE102073) using the GEO query R package, and the ICGC cohort from the ICGC (https://dcc.icgc.org/) database. The normal ovarian tissue data was collected from the GTEx (https://www.gtexportal.org/home/downloads/adult-gtex/overview) database. Regarding scRNA-seq analysis, we enrolled the OV samples from the EMTAB8107 (https://www.ebi.ac.uk/biostudies/arrayexpress/studies/E-MTAB-8107), GSE118828 (https://www.ncbi.nlm.nih.gov/geo/query/acc.cgi?acc=GSE118828), GSE130000 (https://www.ncbi.nlm.nih.gov/geo/query/acc.cgi?acc=GSE130000), and GSE154600 (https://www.ncbi.nlm.nih.gov/geo/query/acc.cgi?acc=GSE154600) cohorts using the TISCH2 database. Data set integration was carried out using the ComBat functions of Sva packages. All data are organized into bulk matrices in TPM format. The TISCH database was used for annotation purposes. Differential gene expression and enrichment pathways of cell subsets were analyzed using the SCP R package. The data employed in this study were exclusively sourced from openly accessible databases, which permit unrestricted downloading and utilization, thereby necessitating no additional ethical approval.

2.2. Collection of TME gene set

Four TME-related gene sets, TMEscoreA_CIR, TMEscoreB_CIR, TMEscoreA_plus, and TMEscoreB_ plus, were found using the signature collection function of the IOBR package.

2.3. Consensus clustering analysis

The unsupervised clustering ConsensusClusterPlus package was used to cluster the OV tumor tissues hierarchically to find two significantly different groups (C1 and C2). PAC scores, CDF curves, and the consensus score matrix were used to determine the optimal number of clusters during the clustering procedure, which was carried out with particular parameters and repetitions.

2.4. Cancer cell stemness analysis

Stemness index evaluation (mRNAsi), which evaluates stem cell gene expression characteristics, was used to evaluate the potential tumor stemness in OV patients. The training dataset includes human stem cell data recruited from the Progenitor Cell Biology Consortium (PCBC) (https://www.synapse.org).

2.5. Machine learning-based model construction

A total of ten different types of machine learning techniques with 101 combinations were used in this study: Elastic net (Enet), Ridge, Lasso, supervised principal components (SuperPC), generalized boosted regression modeling (GBM), random survival forest (RSF), CoxBoost, stepwise Cox regression, and survival support vector machine (survival-SVM). Harrell's concordance index (C-index) was used to assess a model's performance in each dataset; the model with the highest average C-index was selected as the best prognostic model.

2.6. Intratumor immune characterization and drug sensitivity analysis

The TISIDB database (http://cis.hku.hk/TISIDB/) was used to extract information on 150 immunomodulators and chemokines. Among these were 41 chemokines, 24 immuno-inhibitors, 46 immuno-stimulators, 21 MHCs, and 18 receptors. To analyze the immune cell infiltration, the bulk RNA-seq dataset was processed using eight TME analysis algorithms: TIMER, CIBERSORT, EPIC, xCell, ESTIMATE, quanTIseq, MCPcounter, and IPS. These algorithms are integrated into the IOBR R package (https://github.com/IOBR/IOBR). The oncoPredict R package was used to predict drug sensitivity.

2.7. Cell culture

The IOSE80 human ovarian epithelial cell line and the OVCAR3 and SKOV3 ovarian cancer cell lines were acquired from the Shanghai Bank of Cells, part of the Chinese Academy of Science. These cells were grown in DMEM/high glucose medium at 37 °C in a 5 % CO2 environment with a 10 % fetal bovine serum (FBS) supplement.

2.8. Real-time quantitative PCR (RT-qPCR) analysis

The PCR analysis was conducted as previously described [16,17]. Using Trizol reagent (Invitrogen, USA), total RNA was extracted from OVCAR3, SKOV3, and IOSE80 cells. The Mir-X™ miRNA qRT-PCR SYBR® Kit (Takara, Japan) was used to synthesize cDNA in compliance with the manufacturer's instructions. The primers of SH2D1A used for mRNA expression analysis were AGGCGTGTACTGCCTATGTG (forward) and TGCAGAGGTATTACAATGCCTTG (reverse), which was normalized to actin (forward primer: GCCATCTCTTGCTCGAAGTCCAG; reverse primer: ATGTTTGAGACCTTCAACACCCC). Relative gene expression levels were determined using the $2^{-\Delta\Delta Ct}$ method.

2.9. Transwell analysis

The migratory potential of OV cells was assessed using the Transwell assay. An 8 μm pore size transwell insert's upper chamber was seeded with cells at a density of 5×10^4 (Corning, USA). The chamber was maintained at 37 °C for 2 h to promote cell adhesion. The cells were cultured for 24 h, then fixed with 4 % paraformaldehyde and stained using 1 % crystal violet.

2.10. Cell counting kit-8 (CCK8) assay

After being seeded into a 96-well plate, transfected OV cells were treated as described. The culture medium was incubated for 1 h at predefined intervals with 10 L of WST-8 solution (Beyotime Biotech, China). At 450 nm, the cells' absorbance was determined.

2.11. Statistical analysis

For the data processing, statistical analysis, and visualisation in this study, R 4.1.3 software was used. The Pearson correlation coefficient was used to assess the correlation between continuous variables. The study utilized the survival package to conduct Cox and Kaplan-Meier regression analyses to evaluate the association between predictor variables and survival outcomes. These statistical methods provided valuable insights into the associations and prognostic implications of the variables investigated in this study. A statistically significant p-value is defined as $p < 0.05$.

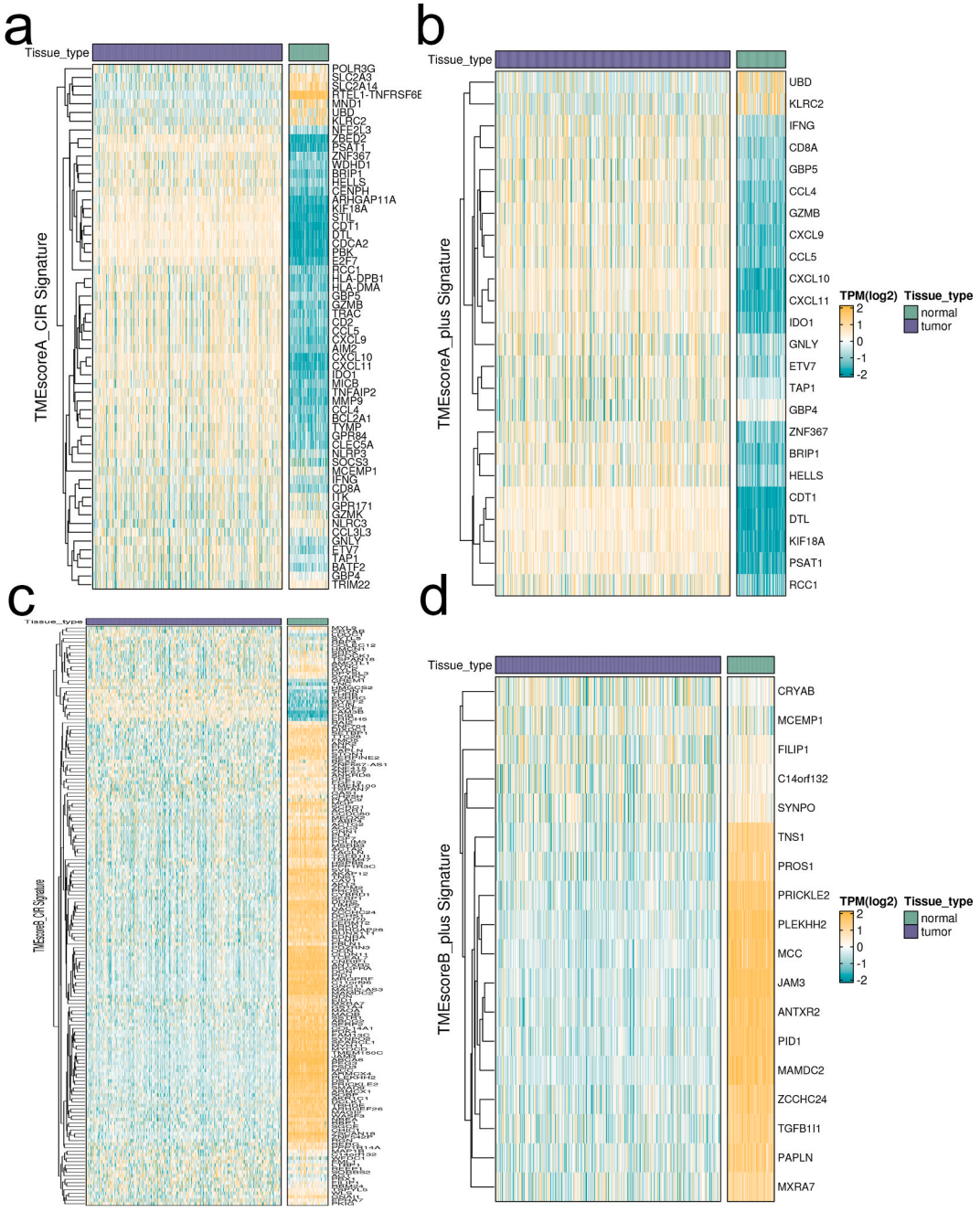

Fig. 1. Expression profiles of TME-related signatures in OV. The expression patterns of four TME-related signatures: (a) TMEscoreA_CIR, (b) TMEscoreA_plus, (c) TMEscoreB_CIR, and (d) TMEscoreB_plus.

3. Results

3.1. Expression profiles of TME-related signatures in OV

To characterize the TME associated phenotypes in the OV cancer, a total of four TME-related gene sets were enrolled. Fig. 1a–d shows all of the TME-related gene's expression patterns. A unanimous elevation of TME-related gene expression could be observed in the TME score A and TME score plus set. However, an opposed expression pattern was found in the TME score B set, suggesting a high intratumor heterogeneity in the OV cancer TME.

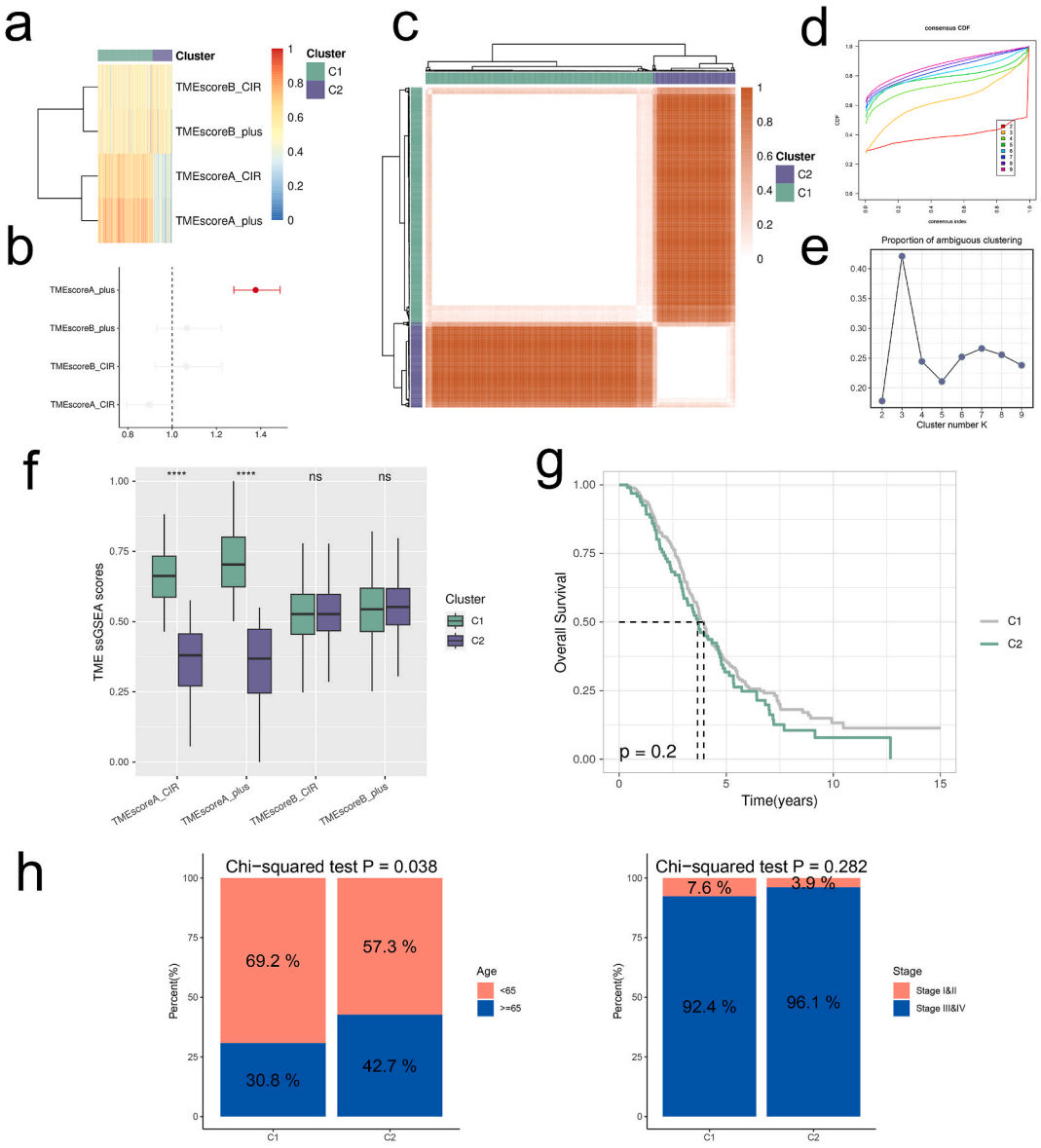

Fig. 2. Distinct TME landscapes in different molecular subclusters of OV patients. (a) The variation in GSVA scores for each TME-related signature between the two TME subclusters (b) The forest plot, which is a product of Univariate Cox regression analysis, shows each TME-related signature's hazard ratio. (c) The OV samples' consensus score matrix in TCGA-OV with k = 2 as the clustering number. The consensus score shows the degree of interaction between the two samples. (d) The CDF curves of the consensus matrix, and (e) the PAC scores for each k-value. (f) Boxplots in the two TME subclusters show the distribution of GSVA scores for each TME-related signature. (g) Kaplan-Meier curves were analyzed, and the survival disparities between the two TME subclusters were assessed using the log-rank test (h). Plots with stacked bars show the age and stage distributions among the TME subclusters. Chi-squared tests were used to get P values.

3.2. Distinct TME landscapes in different molecular subclusters of OV patients

We used the GSVA package to score the four TME-related gene sets in the TCGA-OV data set (Fig. 2a). The forest plot analysis showed that TME score A showed the highest hazard ratio (Fig. 2b). According to the score, unsupervised consensus clustering was used to cluster the OV tumor tissues hierarchically to find two significantly different molecular subgroups (C1 and C2, Fig. 2c–e). Given the highest hazard ratio of TME score A, we calculated TME score A for further analysis. C1 displayed an overall elevation in the TME score A and TME score A plus value, compared to C2, suggesting the C1 group of OV samples was found with higher TME activity (Fig. 2f). However, the overall clinical outcomes of the C1 and C2 clusters did not show any significant differences (Fig. 2g). The C1 group was characterized by a higher proportion of the younger population of OV patients (Fig. 2h). The clinical staging study revealed no significant differences between the C1 and C2 groups.

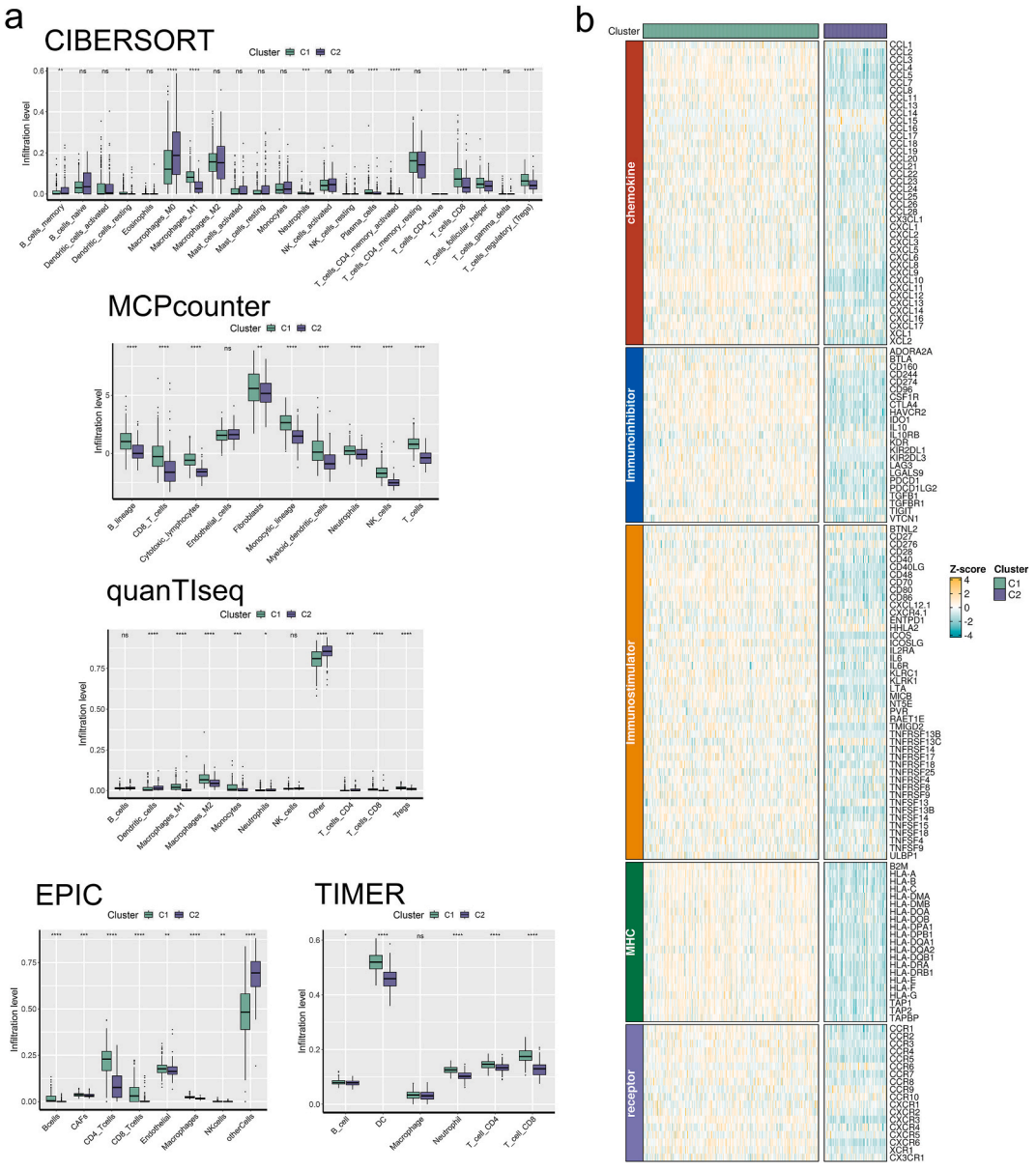

Fig. 3. The C2 TME subcluster shapes a cold-TME in OV. (a) The level of immune cell subset infiltration in the two TME subclusters was measured using CIBERSORT, MCP-counter, quanTIseq, EPIC, and TIMER (b) For each of the two TME subclusters, the immunoregulator expression profiles were analyzed.

3.3. The C2 TME subcluster shapes a cold-TME in OV

To delineate the association between the immune microenvironment and TME of OV cancer, we implemented a series of approaches to characterize the extent of immune infiltration within the OV cancer. M0 and M1 subtypes of macrophages displayed a significantly higher degree of abundance in the C1 subcluster of the OV cancer (Fig. 3a). Consistently, the $CD8^+$ T cells had elevated abundance in the C1 subgroup, suggesting a relatively activated and pro-inflammatory TME in the C1 group. A similar infiltration pattern was found using the MCPcounter and quanTIseq algorithm. Intriguingly, CAFs, regularly deemed one of tumor tumor-facilitating TMEcell groups, were also found to have higher abundances in the C1 group. Moreover, a concurrent expression pattern was found in the chemokine expression levels within the C1 subgroup, probably accounting for the marked elevation in a plethora of intratumor immune cells (Fig. 3b). However, most immune inhibitors, except for IL-10R and KDR, were highly expressed in the C1 subgroup. These results might be attributed to the overall higher number of infiltrated immune cells and/or higher abundance of CAFs in C1. In contrast, a cold TME was identified in C2 OV samples, given lower expression of generally all immune-associated marker genes.

3.4. Drug sensitivity difference between the two TME subclusters

Drug sensitivity analysis in the two TME subclusters showed that the C2 group of OV patients was featured with significantly lower IC50 values of Axitinib, Sorafenib, and Vinblastine, suggesting an overall superior response to these drugs for the C2 group of OV patients (Fig. 4a). On the other hand, C1 group of OV patients may be more beneficial from 5-Fluorouracil. The immune phenotype

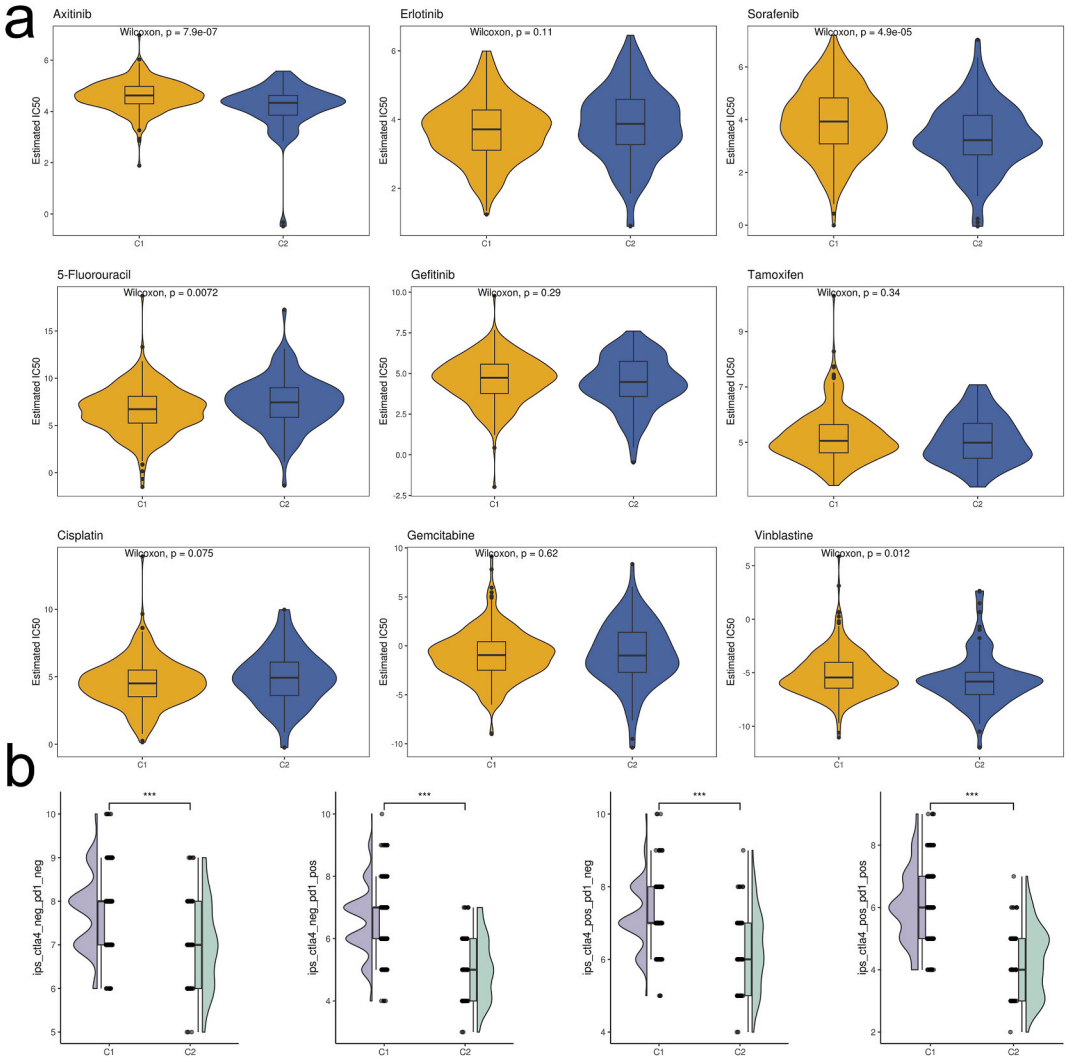

Fig. 4. Drug sensitivity between the two TME subclusters. (a) An illustration of the estimated IC50 values for chemotherapeutic drugs in each of the two TME subclusters using a violin plot. (b) A raincloud plot that compares the two TME subclusters' IPS scores.

score (IPS) analysis showed a higher expression of CTLA4 and PD-1 in the C1 group (Fig. 4b).

3.5. Identification of functional differences between the two TME subclusters

DEGs between C2 and C1 were found using the Limma package and subsequently subjected to enrichment analysis (Fig. 5a). The functional difference between C2 and C1 was mainly found in cell adhesion, mononuclear cell differentiation, and leukocyte migration (Fig. 5b), highly consistent with the elevated abundance of M1 macrophages in the C1 group. GSEA was implemented to identify the differentially activated pathways between C2 and C1. TNF signaling was prominently enriched in the C1 subgroup, suggesting an ongoing cytotoxic activity of C1 OV samples (Fig. 5c). In contrast, mTOR signaling was highly activated in the C2 subgroup, along with notch and TGF-β signaling, presumably exerting immune suppression effects. Because the C2 group had more significantly upregulated DEGs and cold-TME characteristics, WGCNA was used to perform coexpression analysis on the TCGA-OV data set, and three modules significantly related to C2 were found (Fig. 6a–d). Through functional analysis of the interested genes in the 3 mentioned clusters, we found consistent results that C2 was featured with immune response regulatory pathways (Fig. 6e), further suggesting a cold TME within the C2 group of OV samples.

3.6. Machine learning-based TME-related prognostic signature construction

In order to optimize the TME-related prognostic signature construction for OV patients, we combined 10 machine learning methods to select the best algorithm combination in the training set (TCGA-OV) and the test set (2 GEO datasets and 1 ICGC dataset). Stepcox [backward] and RSF had the best prognostic ability (Fig. 7a). The hub genes for prognostic model construction and the corresponding coefficient have been shown in Fig. 7b. CD40LG was identified with the lowest coefficient, suggesting a protective role of CD40LG in OV. In a total of 4 cohorts, including the training set (TCGA-OV) and the test set (2 GEO datasets and 1 ICGC dataset), our TME prognostic model displayed a satisfactory prognosis stratification efficacy across all datasets, featured an AUC value close to 0.8 at different time points (Fig. 7c and d).

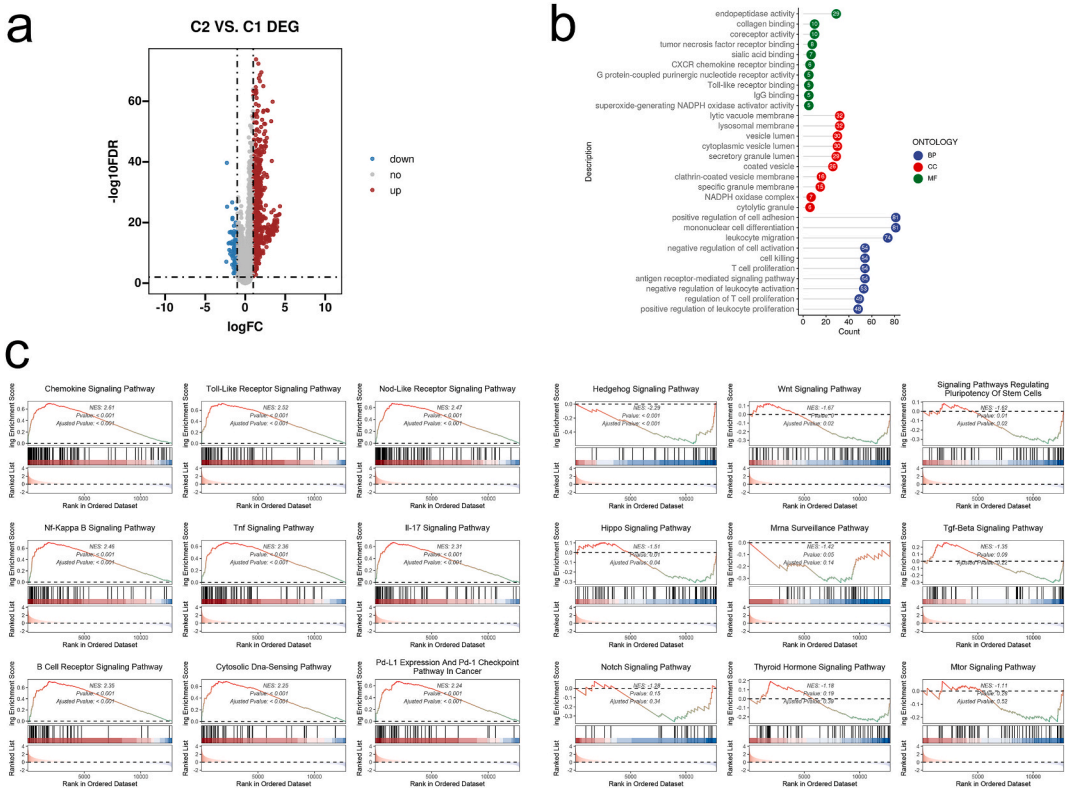

Fig. 5. DEGs between the two TME subclusters. (a) The Volcano plot that compares the two TME subclusters reveals the elevated genes (colored in red) and downregulated (colored in blue). (b) Displayed are the hub genes' top ten enriched GO keywords. (c) GSEA data shows the downregulated pathways on the right panel and the upregulated pathways on the left for the C2 TME subcluster.

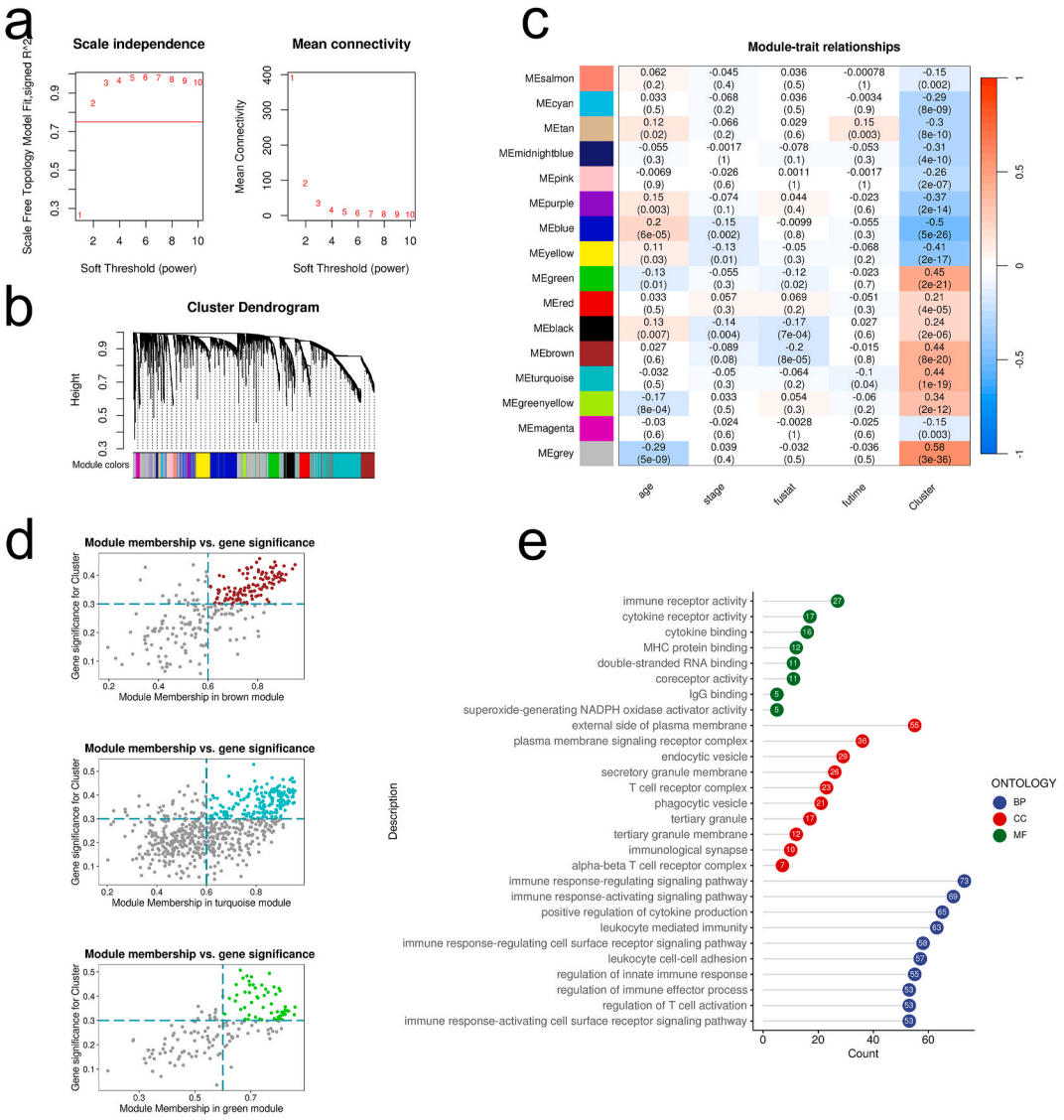

Fig. 6. WGCNA identifies C2-related modules and hub genes inside. (a) Network topology studies across various power levels demonstrate the impacts of a soft-threshold power of 3. The right panel shows how power affects mean connectivity, while the scale-free topology fit index is shown in the left panel. (b) The dendrogram shows the grouping of coexpression modules. Every hue represents a coexpression module. (c) A heatmap illustrating the correlation between module eigengenes and clinical traits (d) The relationship between module membership and the relevance of genes in each of the three modules. For that module, the hub genes were those with colored dots and MM $>$ 0.6 and GS $>$ 0.3. (e) The top ten enriched GO terms for the hub gene.

3.7. Detailed functional landscaping between 2 risk groups of OV patients

In the high-risk group, the total macrophage infiltration was higher, while the M1 macrophages featured with pro-inflammatory characteristics were significantly lower (Fig. 8a). The expression difference of the M2 marker was addressed, showing upregulated expression of IL-10, TGF-β, and CXCR2,4 expression in a high-risk group (Fig. 8b). The T cell exhaustion markers LAG3, PDCD1, and HAVCR2 were strongly elevated in the high-risk OV patients (Fig. 8c), indicating a general immune-suppressive TME in the high-risk group. Moreover, the mRNAs index indicated the general tumor stemness was higher in a high-risk group (Fig. 8d). To provide treatment guidelines for OV patients of different risk values, we observed lower IC50 values in the Dactinomycin, Docetaxel, Dactolisib, and Eg5 in the low-risk group (Fig. 9a). In contrast, high-risk patients might receive a better response from Dasatinib. The IPS analysis is presented in Fig. 9b. Moreover, the high-risk group, characterized by inferior clinical outcomes, was enriched with EMT and hypoxia pathways (Fig. 10).

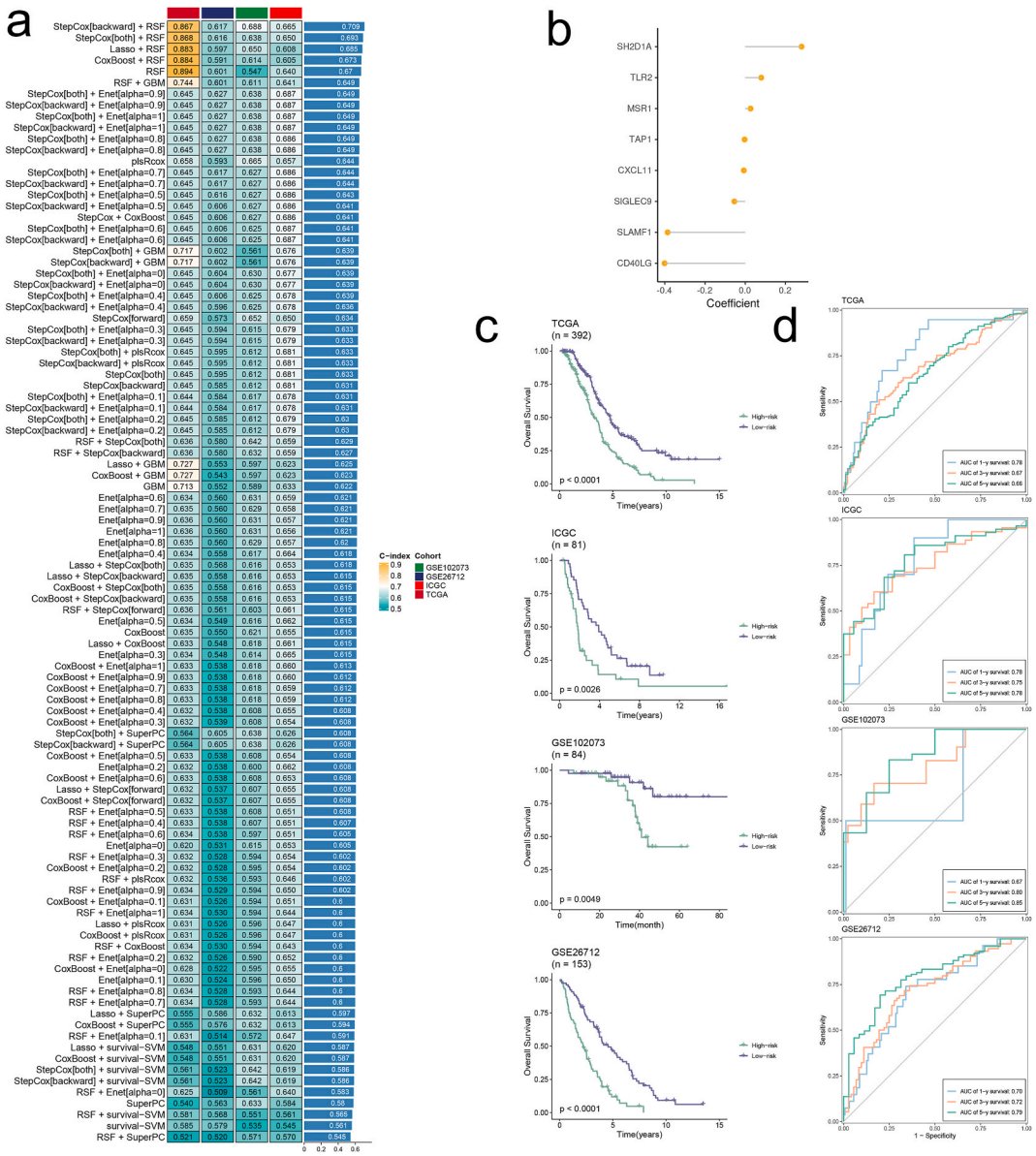

Fig. 7. Machine learning-based TME-related prognostic signature construction. (a) 101 distinct prediction models were developed using TCGA-OV data and validated across three additional cohorts. The average of the C-index across all datasets was used to rank the model. (b): A Lollipop chart displaying the signature gene coefficients ascertained through stepwise Cox regression and RSF. Figure (c): Variations in survival between two groups across the four datasets. (d) shows the model's time-dependent ROC analysis across the four datasets.

3.8. Identification of highly activated TME-related signature in OV

All cells qualified were de-batched and subjected to dimensionality reduction (Fig. 11a). We identified 12 main cell categories (Fig. 11b) using the maker genes presented in Fig. 11c [18]. The up-and-down-regulated genes for each cell group are determined using the SCP pipeline. Compared to identified fibroblasts, activated CAFs had a prominent expression of PDGFRB, SOD3, and PLN (Fig. 11d). The CAFs were found with high extracellular matrix (ECM) formation activity. CD8 T cells were identified as the main cell type, carting out the cytotoxicity towards malignant cells, while macrophages and plasma cells displayed little effect (Fig. 11e). Results from the single-cell analysis of signature gene expression showed that positive TME activity was present in a significant proportion of malignant and CD8 T cells (Fig. 11f).

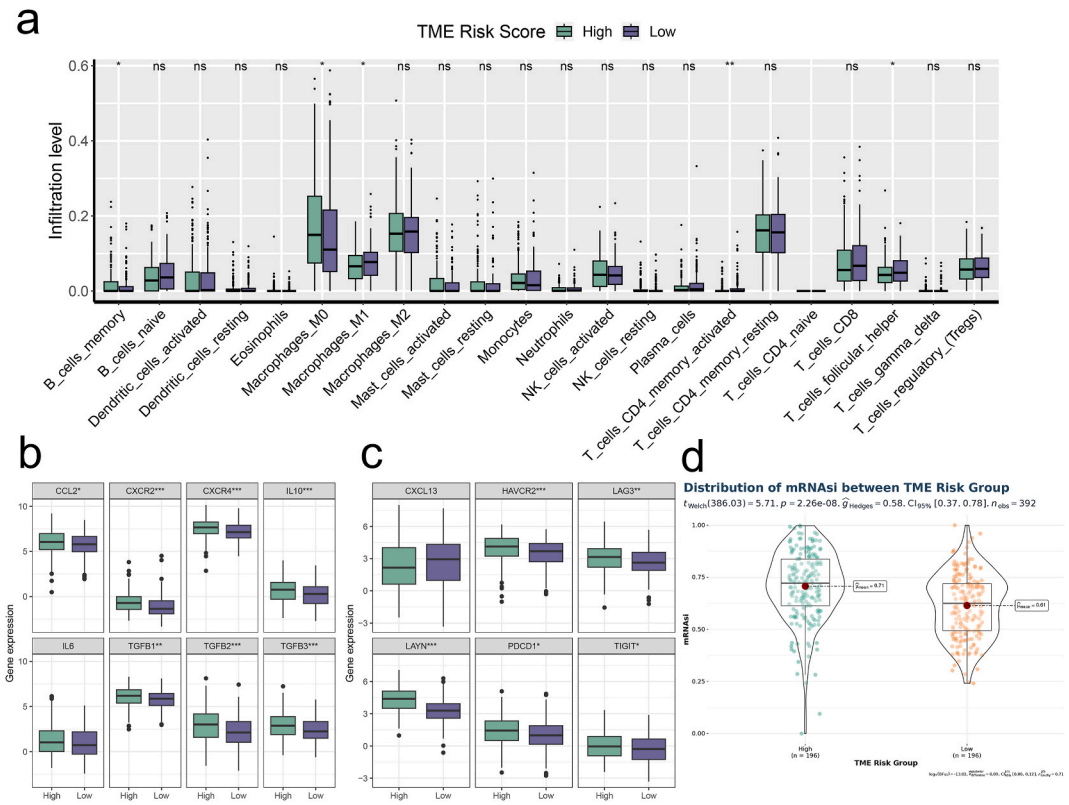

Fig. 8. TME phenotypes between risk groups. (a) In the box plot, we can see how the two risk groups distribute, according to CIBERSORT, 22 different subsets of immune cells. (b) The expression levels of M2 polarization regulators are contrasted between the two risk groups using the box plot. (c) The TEXterm features' expression levels between the two risk groups are shown in another box plot. (d) The mRNAsi index disparities between the two risk groups are shown by a violin plot.

3.9. SH2D1A knockdown contributed to reduced migration and proliferation of OV cancer cell lines

Given that SH2D1A ranked as the top hub gene with the highest coefficient value, we asked whether the loss of SH2D1A could exert a certain influence on OV cancer progression. Using RT-qPCR, we first assessed the mRNA expression of SH2D1A in the human ovarian epithelial cell line IOSE80 and the ovarian cancer cell lines OVCAR3 and SKOV3. The results showed that the levels of SH2D1A mRNA in the cancer cell lines were much higher than those in the normal cell line, indicating a potential role in the disease (Fig. 12a). We used siRNA to conduct knockdown experiments in the OVCAR3 and SKOV3 cell lines to investigate the function of SH2D1A in ovarian cancer cells (Fig. 12b). The effect of SH2D1A knockdown on the rate of proliferation of the OVCAR3 and SKOV3 cell lines was then examined. In comparison to control cells, we observed a significant drop in cell growth at various stages of the cell culture (Fig. 12c). We observed the reduced migratory potential of OVCAR3 and SKOV3 cells with SH2D1A knockdown, reflected by down-regulated transmembrane OV cancer cells (Fig. 12d). This finding suggests that SH2D1A is necessary for ovarian cancer cells to migrate and proliferate.

4. Discussion

This study used computational analysis to explore the role of TME in ovarian cancer. Four TME-related gene sets were analyzed, revealing heterogeneous TME expression patterns. Consensus clustering identified two molecular subgroups with distinct TME activity. The high TME activity subgroup had increased immune infiltration and pro-inflammatory markers. Drug sensitivity analysis showed different responses between subgroups. Functional differences were detected, resulting in the development of a TME-related prognostic signature. Higher tumor stemness and an immune-suppressive TME were present in high-risk patients.

The C1 group of OV samples was observed with higher TME activity, reflected by an increased abundance of M1 macrophages and $CD8^+$ T cells. The infiltration of cytotoxic tumor-infiltrating lymphocytes is considered a positive prognostic biomarker, specifically within the tumor epithelium rather than stromal areas. A compilation of ten studies involving 1815 OV patients reveals that a deficiency of intraepithelial cytotoxic TILs is significantly linked to poorer survival outcomes, with a hazard ratio of 2.24 with a 95 % confidence interval ranging from 1.71 to 2.91 [19]. Improved survival was observed in advanced-stage ovarian cancer patients with higher levels of CD8(+)/FoxP3(+) ratios in tumor tissue, as well as increased CD45R0(+), FoxP3(+), or CD8(+) cytotoxic

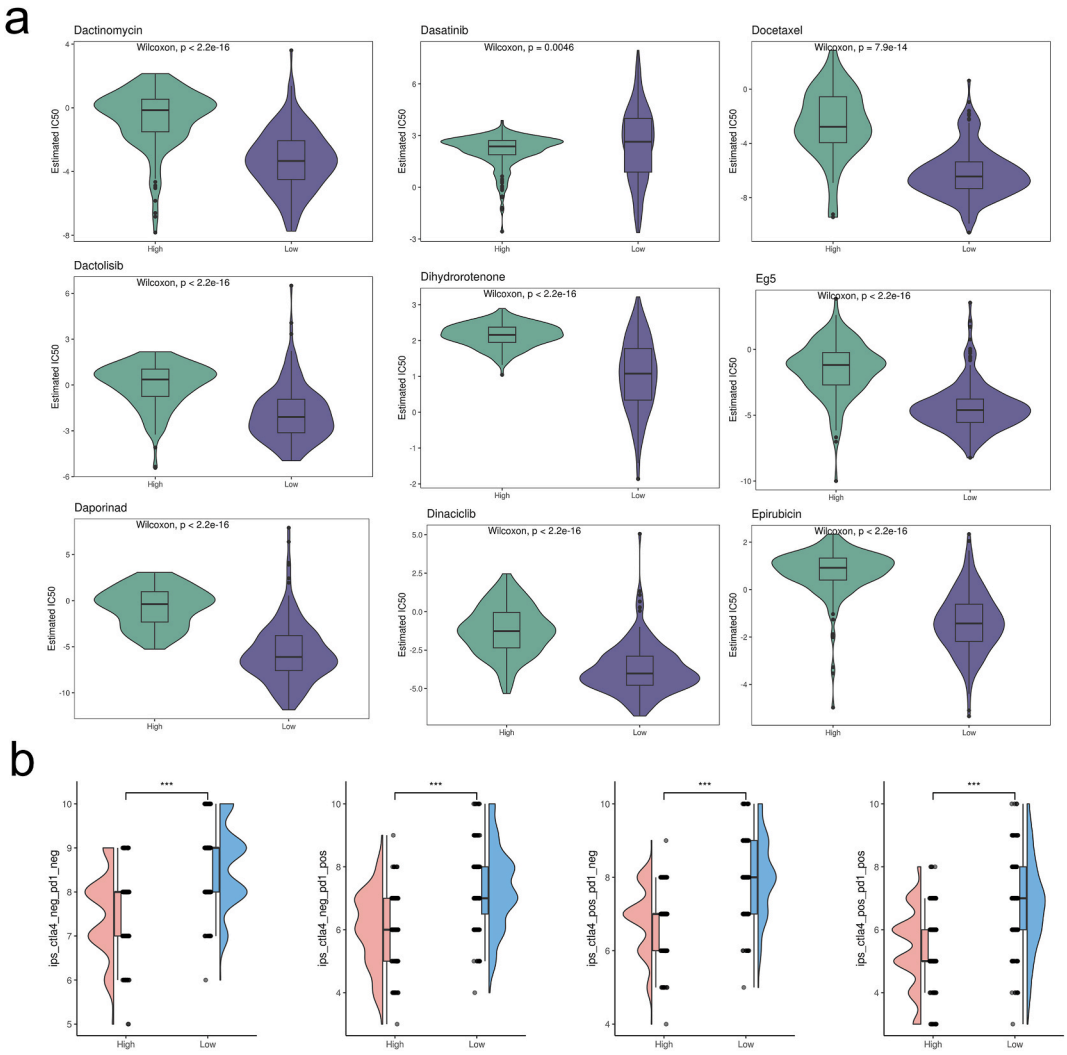

Fig. 9. Therapeutic sensitivity between two risk groups. (a) The violin plot illustrates the distribution of estimated IC50 values for therapeutic agents across the two risk groups. (b) The raincloud plot demonstrates the differences in IPS scores between the two risk groups.

T-lymphocytes in the tumor. A better prognosis was also associated with higher CD45R0(+) memory T-lymphocyte levels in omental metastases [20]. The study's results show that T-lymphocytes in ovarian cancer's primary and metastatic sites improve patient outcomes, particularly in cases of advanced-stage disease. In terms of M1 macrophages, the low-risk group of OV patients and the C1 cluster both showed increased M1 infiltration and a superior prognosis. A high TME ratio of M1 to M2 macrophages is consistently associated with improved survival in patients with ovarian cancer [21]. M1 was widely considered to exert antitumor effects by triggering inflammation within the OV tumors. Thus, many studies were conducted to re-educate M2 into M1 macrophages. TLR 7/8 agonists can potentially repolarize macrophages from an M2 to an M1 state. However, these agonists have limitations, such as off-target effects and poor pharmacokinetic profiles. One of the TLR 7/8 agonists, resiquimod, was loaded into large, anionic liposomes [22]. In murine ovarian cancer models, intraperitoneal administration of these liposomes successfully targeted and repolarized TAMs into the M1 state. Another approach involves targeting specific signaling pathways in ovarian cancer progression and chemoresistance. These processes depend on the NF-kβ signaling pathway, which is regulated by STAT6 and IKKβ. Macrophages can be repolarized from M2-to-M1 both in vivo and in vitro by delivering a STAT6 inhibitor and IKKβ siRNA via a pH-sensitive micellular compound [23].

These findings highlight the potential of utilizing TLR 7/8 agonists in liposomal formulations and targeted inhibition of key signaling pathways to promote macrophage repolarization towards an M1 state. This strategy could have significant implications in developing immunotherapies for improving outcomes in ovarian cancer.

The high expression of T cell exhaustion markers, LAG3, PDCD1, and HAVCR2, in high-risk ovarian cancer patients indicates an immune-suppressive TME in this group. Improved progression-free survival in ovarian cancer has been linked to immune infiltration by $CD8^+$ cytotoxic T cells; recent research suggests that a significant portion of these cells express co-inhibitory molecules, indicating a functionally exhausted state. Poor clinical outcomes and functional exhaustion are associated with the presence of double-positive

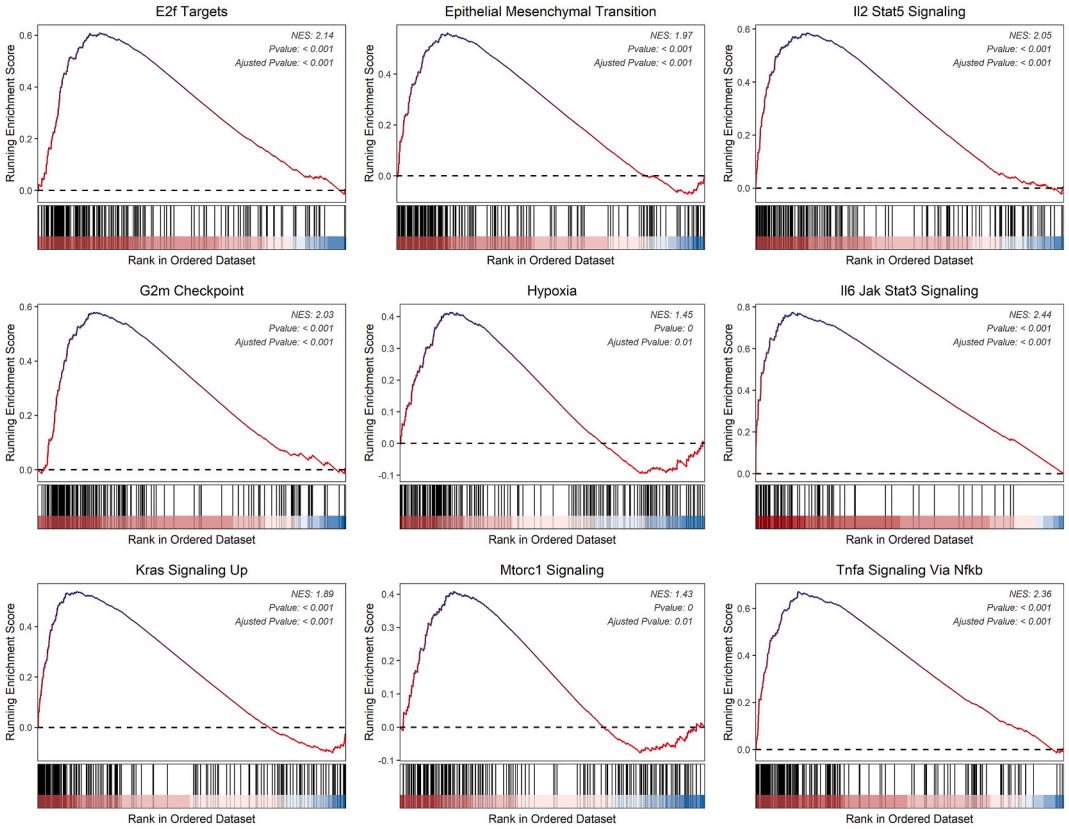

Fig. 10. Dysregulated cancer hallmarks between two risk groups.

$CD8^+$ T cells expressing PD-1 and TIM-3 in high-grade serous ovarian cancer (HGSCs). PD-L1 and TIM-3 are prognostic biomarkers for suppressed immune responses against HGSC [24]. Coexpression of LAG3 and PD1 on T cells invading murine ovarian tumors suggests that these molecules are involved in tumor evasion. Through genetic knockout or antibody blockade, inhibiting both LAG3 and PD1 improved T effector function and delayed the growth of tumors. Additionally, it was found that LAG3 is associated with SHP1/2, which PD1 recruits during T-cell signaling. These results show that the association between LAG3 and PD1 facilitates their trafficking into the OV tumor, which has a mutually synergistic inhibitory effect on T-cell signaling [25]. A higher abundance of $CD8^+$ T cells in OV cancer cells was associated with a higher proportion of mesenchymal cancer cells. LGALS3, associated with EMT, was highly expressed in tumors with EMT phenotypes. Further examination of the tumor microenvironment showed that mesenchymal cancer cells interact with $CD8^+$ T cells via the receptor LAG3, a marker of T cell exhaustion. These findings suggest that EMT in ovarian cancer cells may facilitate interactions between cancer cells and T cells, leading to T cell exhaustion and a diminished immune response to tumors [26]. Using clinical and RNA sequencing expression data, a cohort of 371 OV patients showed that a higher proportion of SPP1 + Tex cells was linked to a poor prognosis. The researchers confirmed that ovarian cancer cells expressed more SPP1 than normal ovarian cells and that suppressing SPP1 promoted apoptosis [27] in tumor cells. Poor survival in HGSC patients was correlated with a novel subpopulation of $CD8^+$ Tex cells that had high expression of TNFRSF1B. Further experiments confirmed that TNFRSF1B upregulation on $CD8^+$ T cells inhibited interferon-γ secretion and was closely correlated with the clinical malignancy of ovarian cancer. Blocking TNFRSF1B also reduced tumor growth and altered the immune microenvironment in a mouse model of ovarian cancer [28]. These findings shed light on potential immune dysfunction mechanisms in ovarian cancer. $CD8^+$ T cells in ovarian cancer can become functionally exhausted, leading to poor disease outcomes. Understanding how co-inhibitory molecules function to attenuate CTL-mediated antitumor immunity could result in the development of novel therapeutic strategies to combat immune exhaustion and enhance the effectiveness of immunotherapies in OV patients.

We found that SH2D1A is a hub gene associated with TMEs in our study, and machine learning analysis gave it the highest coefficient. In the activation of immune cells, SH2D1A is known to play a vital role. Elevated SH2D1A expression in hepatocellular carcinoma (HCC) promoted cell invasion, migration, and proliferation. The Nf-κB signaling pathway was activated, as evidenced by the correlation between this effect and elevated levels of BCL2A1 and p-Nf-κB proteins. SH2D1A expression in HCC was found to be associated with several features of the immune microenvironment. These features include the presence of immune cells, including T cells, B cells, and $CD8^+$ T cells, as well as stromal, ESTIMATE, and immunological scores. Moreover, the expression levels of immune cell markers PDCD1, CD8A, and CTLA4 were found to be correlated with the expression of SH2D1A [29]. SH2D1A protein has been found in Burkitt lymphoma (BL) lines that carry EBV and have a germinal center phenotype. EBV-negative BL lines and those with an

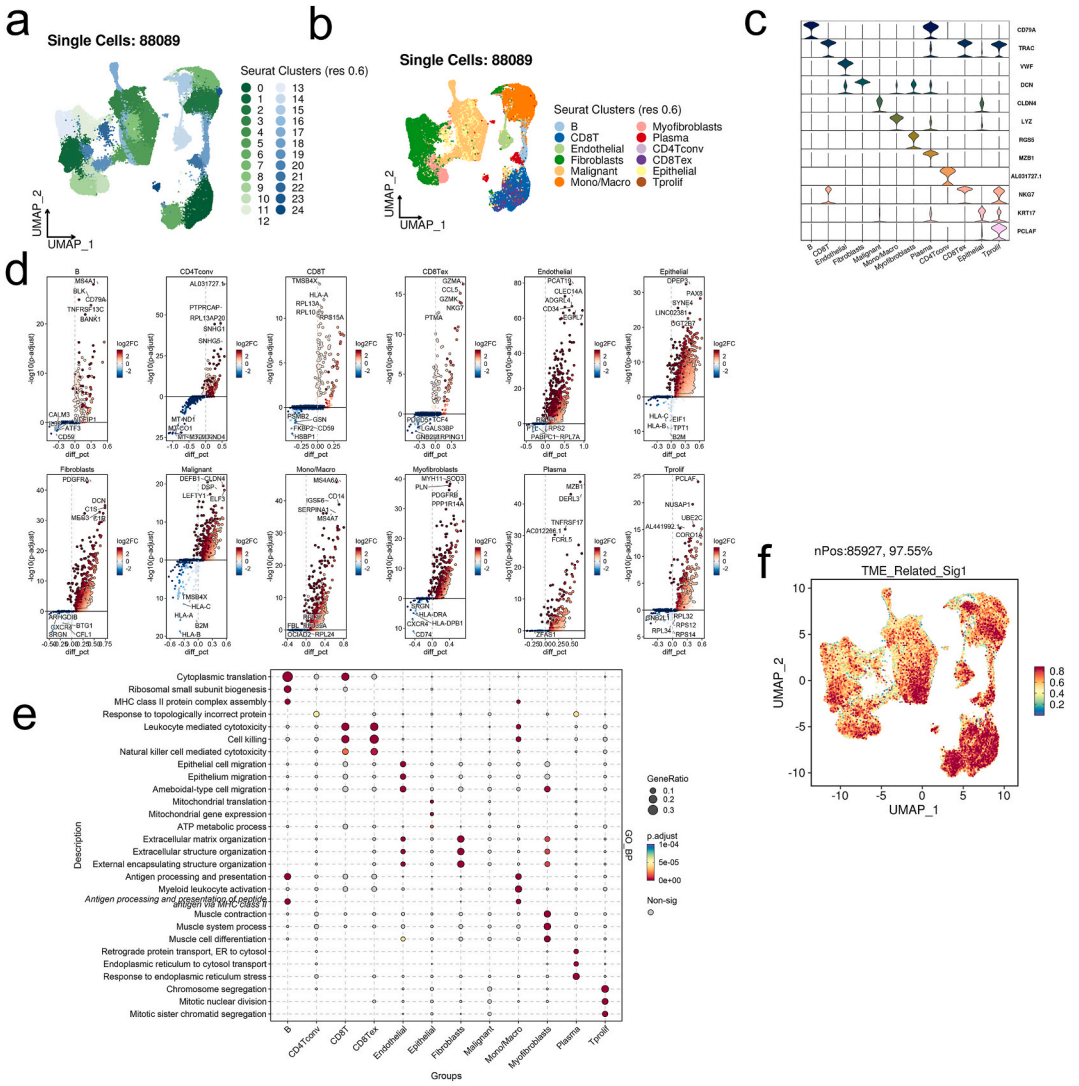

Fig. 11. The highly activated TME-related signature in scRNA-seq datasets of OV. (a) 88,089 cells from four publicly available OV scRNA-seq cohorts visualized using UMAP. (b) A manual annotation of the 12 major cell types was done. (c) Vlnplots that show the marker expression values specific to cell types. (d) The top five labeled markers in each cell cluster are displayed as volcano plots, where the colors blue and red correspond to down- and upregulated, respectively. (e) Dot plot with each cell cluster's enriched GO_BP terms displayed. (f) The AddModuleScore(.) function in Seurat determines the signature gene expression at the single-cell level.

immunoblastic phenotype were SH2D1A-negative [30,31]. However, there is no evidence available to link SH2D1A with OV carcinogenesis. In accordance with our results, these findings suggest that SH2D1A may provide insights into its involvement in OV tumor growth and metastasis, potentially by modulating the immune microenvironment. We found that in two ovarian cancer cell lines (OVCAR3 and SKOV3), SH2D1A knockdown decreased migration and proliferation through a series of in vitro experiments. Cancer cell lines had significantly higher SH2D1A mRNA expression than normal ovarian epithelial cells. Knockdown of SH2D1A reduced cell growth and impaired migratory potential. These findings indicate the important role of SH2D1A in promoting proliferation and migration in ovarian cancer. The results of this study are primarily based on computational analysis and in vitro experiments, lacking large-scale clinical validation. As a result, further confirmation is still needed to determine the data's safety and efficacy in clinical applications. Although the research found that SH2D1A plays an important role in the proliferation and migration of ovarian cancer, our understanding of its specific mechanisms and signaling pathways is still not deep enough. Further study of the molecular mechanisms behind SH2D1A in ovarian cancer is necessary for future research.

5. Conclusion

TME-associated genes were efficient in the molecular subtyping of ovarian cancer. Moreover, a TME-based prognosis model was

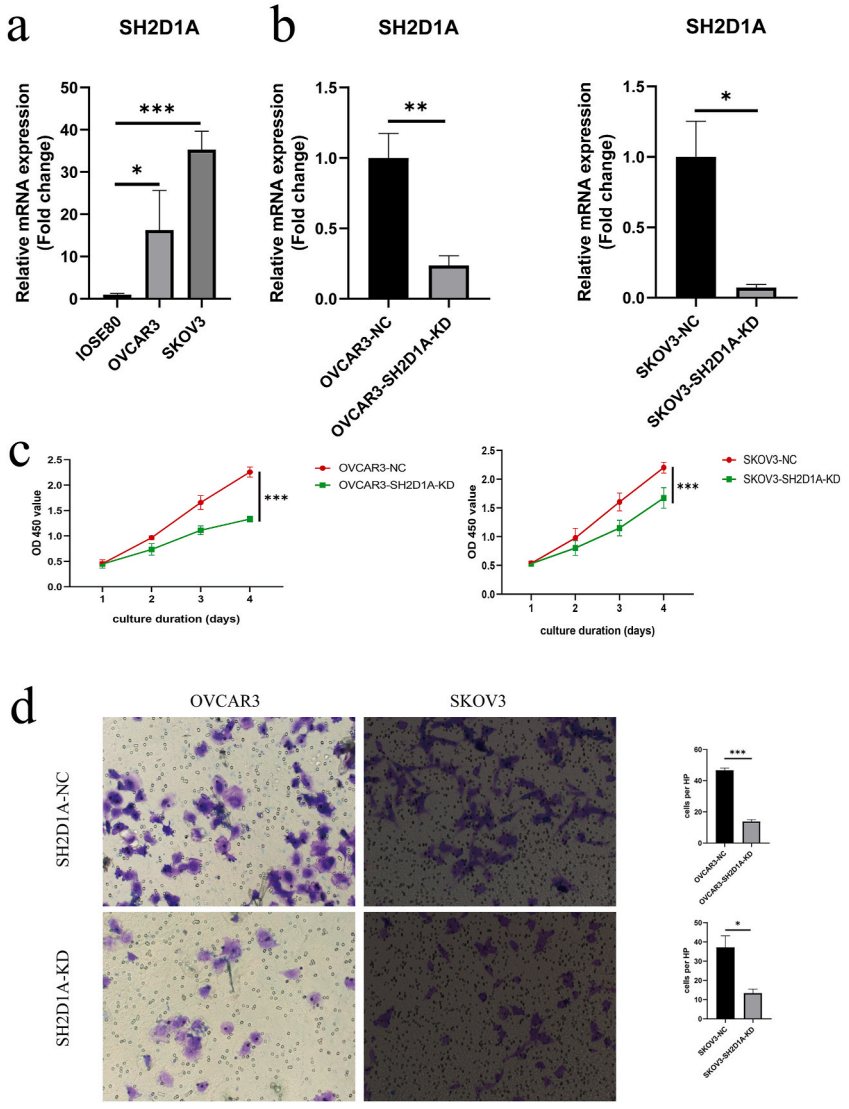

Fig. 12. SH2D1A knockdown contributes to reduced migration and proliferation of OV cancer cell lines. (a) RT-qPCR analysis measured the expression levels of SH2D1A mRNA in the normal human ovarian epithelial cell line IOSE80 and two ovarian cancer cell lines, OVCAR3 and SKOV3. (b) A notable decrease in mRNA expression levels in the ovarian cancer cell lines SKOV3 and OVCAR3 confirmed that SH2D1A knockdown was effective (c) The hampered proliferation rate in the OVCAR3- SH2D1A-KD and SKOV3- SH2D1A-KD cell lines are reflected by reduced OD 450 values. (d) The hampered migratory potential of OVCAR3- SH2D1A-KD and SKOV3- SH2D1A-KD cell lines and corresponding cell counting of 6 different HP. HP, high power lens.

constructed for vigorous prognostic stratification efficacy across multiple datasets. This study provides significant insights into TME of ovarian cancer, including potential therapeutic strategies and prognostic markers.

Ethics

Not application.

Funding

The Shanxi Provincial Health and Family Planning Commission's scientific research project provided funding for this study (2019162).

Data and code availability statement

The original contributions presented in the study are included in the article/supplementary material. Further inquiries can be directed to the corresponding author.

CRediT authorship contribution statement

Hongrui Guo: Writing – original draft, Data curation. **liwen Zhang:** Investigation, Formal analysis. **Huancheng Su:** Project administration, Methodology. **Jiaolin Yang:** Software, Methodology. **Jing Lei:** Formal analysis, Data curation. **Xiaoli Li:** Writing – review & editing. **Sanyuan Zhang:** Writing – review & editing, Formal analysis, Data curation. **Xinglin Zhang:** Writing – review & editing, Writing – original draft, Data curation, Conceptualization.

Declaration of competing interest

The authors declare that they have no known competing financial interests or personal relationships that could have appeared to influence the work reported in this paper.

References

[1] H. Sung, J. Ferlay, R.L. Siegel, M. Laversanne, I. Soerjomataram, A. Jemal, et al., Global cancer Statistics 2020: GLOBOCAN estimates of incidence and mortality worldwide for 36 cancers in 185 countries, CA A Cancer J. Clin. 71 (3) (2021) 209–249.
[2] M. Yu, Y. Wu, Q. Li, W. Hong, Y. Yang, X. Hu, Y. Yang, T. Lu, X. Zhao, X. Wei, Colony-stimulating factor-1 receptor inhibition combined with paclitaxel exerts effective antitumor effects in the treatment of ovarian cancer, Genes Dis 11 (3) (2023 Jun 22) 100989.
[3] L.A. Meyer, W. He, C.C. Sun, H. Zhao, A.A. Wright, R.S. Suidan, et al., Neoadjuvant chemotherapy in elderly women with ovarian cancer: rates of use and effectiveness, Gynecol. Oncol. 150 (3) (2018) 451–459.
[4] L. Dou, E. Lu, D. Tian, F. Li, L. Deng, Y. Zhang, Adrenomedullin induces cisplatin chemoresistance in ovarian cancer through reprogramming of glucose metabolism, Journal of translational internal medicine 11 (2) (2023) 169–177.
[5] M.T. Gyparaki, A.G. Papavassiliou, Epigenetic pathways offer targets for ovarian cancer treatment, Clin. Breast Cancer 18 (3) (2018) 189–191.
[6] D.C. Grossman, S.J. Curry, D.K. Owens, M.J. Barry, K.W. Davidson, C.A. Doubeni, et al., Screening for ovarian cancer: US preventive services task force recommendation statement, JAMA 319 (6) (2018) 588–594.
[7] K. Shen, Q. Wang, L. Wang, Y. Yang, M. Ren, Y. Li, Z. Gao, S. Zheng, Y. Ding, J. Ji, C. Wei, T. Zhang, Y. Zhu, J. Feng, F. Qin, Y. Yang, C. Wei, J. Gu, Prediction of survival and immunotherapy response by the combined classifier of G protein-coupled receptors and tumor microenvironment in melanoma, Eur. J. Med. Res. 28 (1) (2023 Sep 16) 352.
[8] J. Fan, K.K.W. To, Z.S. Chen, L. Fu, ABC transporters affect the tumor immune microenvironment to regulate cancer immunotherapy and multidrug resistance, Drug Resist. Updates 66 (2023 Jan) 100905.
[9] Y. Yang, J. Yang, N. Zhu, H. Qiu, W. Feng, Y. Chen, X. Chen, Y. Chen, W. Zheng, M. Liang, T. Lin, J. Yu, Z. Guo, Tumor-targeting hydroxyapatite nanoparticles for remodeling tumor immune microenvironment (TIME) by activating mitoDNA-pyroptosis pathway in cancer, J. Nanobiotechnol. 21 (1) (2023 Dec 7) 470.
[10] K. Pang, Z.D. Shi, L.Y. Wei, Y. Dong, Y.Y. Ma, W. Wang, G.Y. Wang, M.Y. Cao, J.J. Dong, Y.A. Chen, P. Zhang, L. Hao, H. Xu, D. Pan, Z.S. Chen, C.H. Han, Research progress of therapeutic effects and drug resistance of immunotherapy based on PD-1/PD-L1 blockade, Drug Resist. Updates 66 (2023 Jan) 100907.
[11] Y. He, H. Yu, S. Dai, M. He, L. Ma, Z. Xu, F. Luo, L. Wang, Immune checkpoint inhibitors break whose heart? Perspectives from cardio-immuno-oncology, Genes Dis 11 (2) (2023 Mar 24) 807–818.
[12] J. Gong, A. Chehrazi-Raffle, S. Reddi, R. Salgia, Development of PD-1 and PD-L1 inhibitors as a form of cancer immunotherapy: a comprehensive review of registration trials and future considerations, Journal for immunotherapy of cancer 6 (1) (2018) 8.
[13] H. Su, Y. Wang, H. Li, RNA m6A methylation regulators multi-omics analysis in prostate cancer, Front. Genet. 12 (2021) 768041.
[14] J. Lin, J. Yang, X. Xu, Y. Wang, M. Yu, Y. Zhu, A robust 11-genes prognostic model can predict overall survival in bladder cancer patients based on five cohorts, Cancer Cell Int. 20 (2020) 402.
[15] Y. Liu, Y. Liu, S. Ye, H. Feng, L. Ma, A new ferroptosis-related signature model including messenger RNAs and long non-coding RNAs predicts the prognosis of gastric cancer patients, Journal of translational internal medicine 11 (2) (2023) 145–155.
[16] Z. Xu, Z. Zhou, X. Yang, A. Thakur, N. Han, H.T. Li, L.G. Li, J. Hu, T.F. Li, Y. Yan, Determining M2 macrophages content for the antitumor effects of metal-organic framework-encapsulated pazopanib nanoparticles in breast cancer, J. Nanobiotechnol. 22 (1) (2024 Jul 20) 429.
[17] L. Peikova, Stefan Balkanski, Maya Georgieva, Methods for analysis of fluorinated quinolones in mixtures with nitroimidazole antibacterial drugs, Curr. Pharmaceut. Anal. 18 (2022) 968–982.
[18] W. Shao, Z. Lin, Z. Xiahou, F. Zhao, J. Xu, X. Liu, P. Cai, Single-cell RNA sequencing reveals that MYBL2 in malignant epithelial cells is involved in the development and progression of ovarian cancer, Front. Immunol. 15 (2024 Jul 29) 1438198.
[19] N. Liu, D. Li, D. Liu, Y. Liu, J. Lei, FOSL2 participates in renal fibrosis via SGK1-mediated epithelial-mesenchymal transition of proximal tubular epithelial cells, Journal of translational internal medicine 11 (3) (2023) 294–308.
[20] W.T. Hwang, S.F. Adams, E. Tahirovic, I.S. Hagemann, G. Coukos, Prognostic significance of tumor-infiltrating T cells in ovarian cancer: a meta-analysis, Gynecol. Oncol. 124 (2) (2012) 192–198.
[21] N. Leffers, M.J. Gooden, R.A. de Jong, B.N. Hoogeboom, K.A. ten Hoor, H. Hollema, et al., Prognostic significance of tumor-infiltrating T-lymphocytes in primary and metastatic lesions of advanced stage ovarian cancer, Cancer Immunol. Immunother. : CII. 58 (3) (2009) 449–459.
[22] Y. Yousefzadeh, S. Hallaj, M. Baghi Moornani, A. Asghary, G. Azizi, M. Hojjat-Farsangi, et al., Tumor associated macrophages in the molecular pathogenesis of ovarian cancer, Int. Immunopharm. 84 (2020) 106471.
[23] Y. Kang, L. Flores, H.W. Ngai, Y.R. Cornejo, T. Haber, M. McDonald, et al., Large, anionic liposomes enable targeted intraperitoneal delivery of a TLR 7/8 agonist to repolarize ovarian tumors' microenvironment, Bioconjugate Chem. 32 (8) (2021) 1581–1592.
[24] H. Xiao, Y. Guo, B. Li, X. Li, Y. Wang, S. Han, et al., M2-Like tumor-associated macrophage-targeted codelivery of STAT6 inhibitor and IKKβ siRNA induces M2-to-M1 repolarization for cancer immunotherapy with low immune side effects, ACS Cent. Sci. 6 (7) (2020) 1208–1222.
[25] J. Fucikova, J. Rakova, M. Hensler, L. Kasikova, L. Belicova, K. Hladikova, et al., TIM-3 dictates functional orientation of the immune infiltrate in ovarian cancer, Clin. Cancer Res. : an official journal of the American Association for Cancer Research 25 (15) (2019) 4820–4831.
[26] R.Y. Huang, C. Eppolito, S. Lele, P. Shrikant, J. Matsuzaki, K. Odunsi, LAG3 and PD1 co-inhibitory molecules collaborate to limit CD8+ T cell signaling and dampen antitumor immunity in a murine ovarian cancer model, Oncotarget 6 (29) (2015) 27359–27377.
[27] E. Yakubovich, D.P. Cook, G.M. Rodriguez, B.C. Vanderhyden, Mesenchymal ovarian cancer cells promote CD8(+) T cell exhaustion through the LGALS3-LAG3 axis, NPJ systems biology and applications 9 (1) (2023) 61.
[28] K. Wang, H. Hou, Y. Zhang, M. Ao, H. Luo, B. Li, Ovarian cancer-associated immune exhaustion involves SPP1+ T cell and NKT cell, symbolizing more malignant progression, Front. Endocrinol. 14 (2023) 1168245.

[29] Y. Gao, H. Shi, H. Zhao, M. Yao, Y. He, M. Jiang, et al., Single-cell transcriptomics identify TNFRSF1B as a novel T-cell exhaustion marker for ovarian cancer, Clin. Transl. Med. 13 (9) (2023) e1416.
[30] Q.M. Xiang, N. Jiang, Y.F. Liu, Y.B. Wang, D.A. Mu, R. Liu, et al., Overexpression of SH2D1A promotes cancer progression and is associated with immune cell infiltration in hepatocellular carcinoma via bioinformatics and in vitro study, BMC Cancer 23 (1) (2023) 1005.
[31] N. Nagy, A. Maeda, K. Bandobashi, L.L. Kis, J. Nishikawa, P. Trivedi, et al., SH2D1A expression in Burkitt lymphoma cells is restricted to EBV positive group I lines and is downregulated in parallel with immunoblastic transformation, Int. J. Cancer 100 (4) (2002) 433–440.